Langmuir Article

pubs.acs.org/Langmuir

A Simple and Efficient Method Using Polymer Dispersion To Prepare Controllable Nanoporous TiO_2 Anodes for Dye-Sensitized Solar Cells

Jiaoli Li,[†] Liduo Wang,*[,†] Xiangming Kong,[‡] Beibei Ma,[†] Yantao Shi,[†] Chun Zhan,[†] and Yong Qiu*[,†]

[†]*Key Lab of Organic Optoelectronics & Molecular Engineering of the Ministry of Education, Department of Chemistry, Tsinghua University, Beijing 100084, China, and* [‡]*Department of Civil Engineering, Tsinghua University, Beijing 100084, China*

Received April 27, 2009. Revised Manuscript Received June 9, 2009

An efficient method using a polymer dispersion (PD) based on a copolymer of styrene and butyl acrylate to prepare TiO_2 electrodes for dye-sensitized solar cells (DSCs) was introduced. The obtained TiO_2 nanoporous film was investigated by scanning electron microscopy (SEM) and Brunauer−Emmett−Teller (BET) analysis. A porous structure with pore size distribution from tens of nanometers to several hundred nanometers or even micrometers was characterized. This offered the film a feature of high haze factor and porosity. When using the film as photoanode, a quasi-solid-state DSC was successfully fabricated. The device showed an improved per-weight-efficiency by a factor of 2.7, resulting from the reduced interfacial resistance and the enhanced light scattering effect revealed by electrochemical impedance spectroscopy and transmittance spectroscopy, respectively. The developed PD-based colloid is promising to be applied in production on a large scale as a result of its simple prescription and stability during storage. A proposal to further improve the porous film is also introduced at the end of the paper.

Introduction

Photovoltaic devices are potentially one of the most important emerging new technologies, since the harvesting of energy by solar cells promises to be of increasing necessity as our reserves of fossil fuels dwindle. Dye-sensitized solar cells (DSCs) have received a lot of attention as low cost alternatives to conventional semiconductor photovoltaic devices.[1−4] The DSCs consist of a dye adsorbed on a nanoporous film prepared from nanoparticles of metal oxide, typically TiO_2 as the electron transporter, an electrolyte as a hole transport layer, and the counter electrode for collection of holes.[5] Among these, the porous film with sufficient surface area is the key factor in the optimization of DSC, because of the low absorbance of dye monolayers and the low efficiency of dye multilayers.[6] The well-applied method for preparation of TiO_2 film employs nanosize semiconductor colloid, which is composed of TiO_2 nanoparticles and additives. The colloid is succeedingly sintered on a transparent conducting substrate, thus forming a porous geometry.[7] The adopted additives are water for dispersing the nanoparticles, acetylacetone for preventing the reaggregation, detergent (Triton X-100) for facilitating the spreading of the colloids on the substrate, and polymers for forming pores. These components are added into the colloid step by step, which is potentially a disadvantage for large-scale production compared to a one-pot method. In this paper, an efficient method, featuring a one-pot and simplified prescription, is introduced.

In order to enhance the light absorption capability of TiO_2 film, efforts have been devoted to the development of more efficient photoanode materials[8−15] in addition to the use of new near-infrared dyes.[15−22] One strategy is to employ an additional scattering layer in the photoanode, for example, a multilayer with gradually increasing TiO_2 particles, that is, three layers of 16 nm, 25 nm, and 300 nm.[23] However, the improvement is often limited because of the decreased surface area compared to a nanoparticle

*To whom correspondence should be addressed. E-mail: chldwang@mail.tsinghua.edu.cn.

(1) O'Regan, B.; Grätzel, M. *Nature* **1991**, *353*, 737–740.
(2) Asbury, J. B.; Ellingson, R. J.; Gosh, H. N.; Ferrere, S.; Notzig, A. J.; Lian, T. *J. Phys. Chem. B* **1999**, *103*, 3110–3119.
(3) Park, N. G.; Kang, M. G.; Kim, K. M.; Ryu, K. S.; Chang, S. H.; Kim, D. K.; Van de Lagemaat, J.; Benkstein, K. D.; Frank, A. J. *Langmuir* **2004**, *20*, 4246–4253.
(4) Furube, A.; Katoh, R.; Yoshihara, T.; Hara, K.; Murata, S.; Arakawa, H.; Tachiya, M. *J. Phys. Chem. B* **2004**, *108*, 12588–12592.
(5) Kubo, W.; Murakoshi, K.; Kitamura, T.; Yoshida, S.; Haruki, M.; Hanabusa, K.; Shirai, H.; Wada, Y.; Yanagida, S. *J. Phys. Chem. B* **2001**, *105*, 12809.
(6) Hagfeldt, A.; Grätzel, M. *Chem. Rev.* **1995**, *95*, 49–68.
(7) Nazeeruddin, M. K.; Kay, A.; Roicio, I.; Baker, R. H.; Müller, E.; Liska, P.; Vlachopoulos, N.; Grätzel, M. *J. Am. Chem. Soc.* **1993**, *115*, 6382–6390.
(8) Chappel, S.; Chen, S. G.; Zaban, A. *Langmuir* **2002**, *18*, 3336–3342.
(9) Adachi, M.; Murata, Y.; Takao, J.; Jiu, J.; Sakamoto, M.; Wang, F. *J. Am. Chem. Soc.* **2004**, *126*, 14943–14949.
(10) Law, M.; Greene, L. E.; Johnson, J. C.; Saykally, R.; Yang, P. D. *Nat. Mater.* **2005**, *4*, 455–459.
(11) Zukalová, M.; Zukal, A.; Kavan, L.; Nazeeruddin, M. K.; Liska, P.; Grätzel, M. *Nano Lett.* **2005**, *5*, 1789–1792.
(12) Zhu, K.; Neale, N. R.; Miedaner, A.; Frank, A. J. *Nano Lett.* **2007**, *7*, 69–74.
(13) Kim, D.; Ghicov, A.; Albu, S. P.; Schmuki, P. *J. Am. Chem. Soc.* **2008**, *130*, 16454–16455.
(14) Yang, L.; Lin, Y.; Jia, J. G.; Xiao, X. R.; Li, X. P.; Zhou, X. W. *J. Power Sources* **2008**, *182*, 370–376.
(15) Kuang, D.; Brillet, J.; Chen, P.; Takata, M.; Uchida, S.; Miura, H.; Sumioka, K.; Zakeerudin, S. M.; Grätzel, M. *ACS Nano* **2008**, *2*, 1113–1116.
(16) Sayama, K.; Tsukagoshi, S.; Hara, K.; Ohga, Y.; Shinpou, A.; Abe, Y.; Suga, S.; Arakawa, H. *J. Phys. Chem. B* **2002**, *106*, 1363–1371.
(17) Hara, K.; Sato, T.; Katoh, R.; Furube, A.; Ohga, Y.; Shinpo, A.; Suga, S.; Sayama, K.; Sugihara, H.; Arakawa, H. *J. Phys. Chem. B* **2003**, *107*, 597–606.
(18) Horiuchi, T.; Miura, H.; Sumioka, K.; Uchida, S. *J. Am. Chem. Soc.* **2004**, *126*, 12218–12219.
(19) Kim, S.; Lee, J. K.; Kang, S. O.; Ko, J.; Yum, J. H.; Fantacci, S.; De Angelis, F.; DiCenso, M. D.; Nazeeruddin, K.; Grätzel, M. *J. Am. Chem. Soc.* **2006**, *128*, 16701–16707.
(20) Kuang, D.; Walter, P.; Nesch, F.; Kim, S.; Ko, J.; Comte, P.; Zakeeruddin, S. M.; Nazeeruddin, M. K.; Grätzel, M. *Langmuir* **2007**, *23*, 10906–10909.
(21) Hagberg, D. P.; Yum, J. H.; Lee, H. J.; De Angelis, F.; Marinado, T.; Karlsson, K. M.; Baker, R. H.; Sun, L.; Hagfeldt, A.; Grätzel, M.; Nazeeruddin, M. K. *J. Am. Chem. Soc.* **2008**, *130*, 6259–6266.
(22) Y., J. H.; Jang, S. R.; Humphry-Baker, R.; Grätzel, M.; Cid, J. J.; Torres, T.; Nazeeruddin, M. K. *Langmuir* **2008**, *24*, 5636–5640.
(23) Hu, L. H.; Dai, S. Y.; Weng, J.; Xiao, S. F.; Sui, Y. F.; Huang, Y.; Chen, S. H.; Kong, F. T.; Pan, X.; Liang, L. Y.; Wang, K. J. *J. Phys. Chem. B* **2007**, *111*, 358–362.

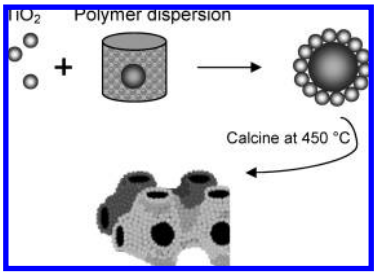

Figure 1. Illustration of a PD-based colloid (PD colloid) for the preparation of TiO_2 porous films S1 and S2.

device. Another way is to incorporate scattering centers in the TiO_2 layer. More recently, the improved light-harvesting efficiency was reported for DSCs using nanotube TiO_2[12] or nanoembossed hollow spherical TiO_2 particles.[24−26] The main contributing factors were the extension of the light path length and the decrease in the transport resistance. The disadvantage is that the multistep synthesis, which is often necessary in the preparation of nanotubes and hollow spheres, limits the realization of large-scale production. The possible substitute is nanoparticle film containing big voids as the light scattering center. In 2005, Hore successfully fabricated TiO_2 porous film using carboxyl-stabilized polystyrene (PS) particles with a diameter of 400 nm as the pore-forming agent.[27] The liquid cell composed by the nanoparticles films with diameters of 20−25 nm incorporated with additional big TiO_2 particles with diameters of 150−300 nm showed an improved performance by 25%. Our paper proposes another easier strategy to produce positively controllable porous TiO_2 films for DSCs, which involves the introduction of a polymer dispersion (PD), other than PS particles as the pore-forming agent.

PD is well-known as commercialized products applied in many industrial fields, such as in coatings, adhesives and paints. Its production through emulsion polymerization is well developed, which is characterized with low cost, diverse properties, and huge throughput. Direct use as bought of a PD in the preparation of TiO_2 porous films provides an easy and cheap possibility to reduce the production cost of the solar cells. A typical PD is composed of polymer particles dispersing evenly in an aqueous solution with particle size ranging from tens of nanometer to micrometers. After blended with TiO_2 nanoparticles, the bigger polymer particles could be encapsulated by TiO_2 nanoparticles as a result of the static force and the tendency of minimization of interface energy, as illustrated in Figure 1.

The PD colloid containing the self-organized bilayer particles is then deposited onto the conductive substrate by a doctor-blading technique. The organic components are removed by the succeeding thermal treatment at 450 °C in air, resulting in an interconnected network composed of the TiO_2 shell. By modulating the content of TiO_2 and polymer particles, a bicontinuous network is expected to set up. This network can provide the percolation pathways for charges and electrons on one hand, and on the other hand, a large interfacial area for adsorption of dyes and for charge injection to the hole conductor. Figure 1 gives an ideal bicontinuous model. However, collapse of the shell may happen during the thermal solidification induced by gravity force. Although this phenomenon leads to a deviation of morphology from the ideal structure, it can improve the mechanical property to ensure the fabrication of the solar cell.

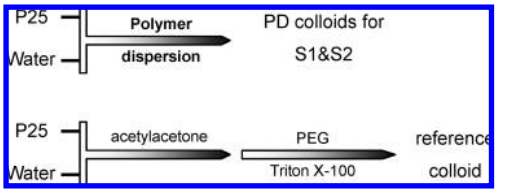

Figure 2. Scheme of preparation of the colloid using PD (top). The reference colloid is also shown on the bottom for comparison.

Here, a PD based on a copolymer of styrene and butyl acrylate is used in this work. Compared to the PS particles, the copolymerization of styrene with other monomer such as butyl acrylate provides possibilities to tune the properties of the copolymer particle by adjusting the copolymerization ratio of the two monomers. Therefore, the hardness of the copolymer particles and the polarity of the particle surface could vary in a large range from very hard and unpolar to soft and polar. The glass transition temperature (T_g) of the copolymer can be varied in the range of −40 to 100 °C. This supplies an optimized interaction between TiO_2 particles and polymer particles, consequently optimizing the morphology of the TiO_2 films. At the end of this paper, a porous film with high haze factor is obtained without the use of big TiO_2 particles. By taking this porous film as the photoanode, the corresponding quasi-solid-state DSC shows a greatly improved per-weight-efficiency, which is carefully discussed with results from electrochemical impedance spectroscopy (EIS) and transmittance spectroscopy.

Experimental Section

Preparation of the TiO_2 Film. Two PDs, D1 and D2, which contain a copolymer of styrene and butyl acrylate, were used as bought from BASF. Both samples have the same T_g of about 20 °C. The particle size distribution was characterized by dynamic laser scattering (DLS) measurement, as shown in Figure 5, which indicates a characteristic particle size of 200 nm for D1 and 500 nm for D2, respectively. The solid content of both D1 and D2 are 50 wt %. The PD colloids were prepared by thoroughly mixing TiO_2 nanoparticles (Degussa P25), PD, and water. For the D1 colloid, 3.94 g P25 were dispersed in the mixture of 8.75 g of D1 and 20 mL of H_2O. For the D2 colloid, 2.67 g of P25 were dispersed in the mixture of 7 g of D2 and 15.2 mL H_2O. The mixture was stirred for 24 h at room temperature (RT) to achieve a homogeneous colloid. The reference colloid was prepared using the same method as reported before.[28] The blend of 3 g of P25, 17 mL of H_2O, and 0.27 mL of acetylacetone were ultrasonically bathed before 0.13 mL of Triton X-100, 0.75 g of poly(ethylene glycol) (PEG; $M_n = 2 \times 10^4$ g/mol), and 0.15 g of PEG ($M_n = 2 \times 10^6$ g/mol) were added, followed by stirring at RT for 24 h. The colloid was then deposited onto the precleaned fluorinated tin oxide (FTO) glass by the technique of doctor-blading. The films were succeedingly treated at 450 °C in air atmosphere for 30 min to remove the organic components, thus producing the porous TiO_2 films. The preparation scheme is shown in Figure 2. The reference method was also given on the bottom.

DSC Fabrication and Testing. The above obtained TiO_2 films were soaked in a 3×10^{-4} M solution of N3 (Solaronix) in ethanol overnight. Devices S1 and S2 used the photoanode prepared from the D1 and D2 colloids, respectively. The quasi-solid-state device was then fabricated by using a quasi-solid-state

(24) Koo, H. J.; Kim, Y. J.; Lee, Y. H.; Lee, W. I.; Kim, K.; Park, N. *Adv. Mater.* **2008**, *20*, 195–199.
(25) Kondo, Y.; Yoshikawa, H.; Awaga, K.; Murayama, M.; Mori, T.; Sunada, K.; Bandow, S.; Lijima, S. *Langmuir* **2008**, *24*, 547–550.
(26) Nelson, K.; Deng, Y. *Langmuir* **2008**, *24*, 975–982.
(27) Hore, S.; Nitz, P.; Vetter, C.; Prahl, C.; Niggemann, M.; Kern, R. *Chem. Commun.* **2005**, 2011–2013.
(28) Luo, F.; Wang, L. D.; Ma, B. B.; Qiu, Y. *J. Photochem. Photobiol. A: Chem.* **2008**, *197*, 375–381.

polymer electrolyte as reported before.[29] The AM1.5 solar simulator (Xenon lamp, Oriel) was used as the light source, with the incident light intensity calibrated by a standard crystalline silicon solar cell. Current−wavelength ($I-\lambda$) curves were recorded with a Keithley 4200 Source-Measurement Unit. The active area of the DSC was 0.25 cm^2 defined by a black mask.

Characterization. The particle size distribution of the PD was measured by DLS (Malvern Mastersizer 2000). Scanning electron microscopy (SEM; FEI Quanta 200 FEG, Holland) and transmission electron microscopy (TEM; JEOL 200CX, Japan) were performed to observe the morphology of the self-organized particles and the calcinated TiO_2 film. For the SEM sample, a thin layer of carbon was deposited for a better conductivity. The porous structure of the TiO_2 film, characterized by pore size distribution and porosity, was determined by a high pressure porosimeter (Quantachrome, Autoscan-33) using mercury as the medium. The transmittance spectra were taken with a HITACHI UV spectrophotometer (model U-3010UV) fitted with a 10 cm diameter integrating sphere coated with polytetrafluoroethylene (PTFE). The sample was placed at the entrance port for transmittance measurements. The exit port was covered with a diffuse PTFE reflector for recording the total transmittance T_{total}. The diffuse transmittance T_d was measured with an open exit port, allowing the collimated part of the transmitted beam to cross the sphere. The collimated transmittance was calculated from the difference of the total and the diffuse transmittance. The haze factor was calculated from the formula of haze factor = T_d/T_{total}. To analyze the internal resistance of the DSC, EIS measurement (CHI660 electrochemical workstation, USA) was carried out with a signal frequency ranging from 0.05 Hz to 100 kHz in full sunlight (100 mW/cm^2). The working electrode was a dye-sensitized TiO_2 film of DSCs. The auxiliary electrode and the reference electrode were a platinized conducting glass of DSCs. Finally, the amplitude of the alternative signal was 100 mV, and an open circuit voltage (Voc) was applied as the bias voltage so that there was no electric current flowing.

Results and Discussion

The self-organization behavior of polymer particles and TiO_2 nanoparticles was investigated by TEM. It is known that the surface modification of organic materials can be carried out in order to achieve good anchoring to TiO_2. For example, carboxyl-stabilized PS spheres served as pore forming agents in the preparation of porous TiO_2 film.[27] Here, the copolymer of styrene and butyl acrylate is used to prepare the spherical voids in TiO_2 film. The introduction of butyl acrylate increases the polarity of the polymer, thus enhancing the molecular interaction between TiO_2 and polymer particles. A close encapsulation of polymer particles by TiO_2 nanoparticles is obtained (Figure 3). Furthermore, flexible control on the thermal properties of the copolymer can be easily realized by varying the ratio of the styrene unit and the butyl acrylate unit. The copolymer used in this work has a T_g of 20 °C, which offers a suitable surface for adhesion of TiO_2. As shown in the inset of Figure 3a, the polymer particles show less color contrast than the TiO_2 nanoparticles as a result of the lower density of the polymer. The size and shape of the polymer particles do not change, as they apparently displace their surroundings of water by air because of the higher T_g above RT. This leads to a successful transition of the self-organization behavior from the colloid to a solid film. For S1 and S2, the TiO_2 nanoparticles are attached onto the surface of the polymer particles, forming a double-layered sphere (Figure3). The sphere varies in diameter for D1 and D2, which are approximately 200 and 500 nm, respectively. Some free TiO_2 nanoparticles are also seen because of the high content of TiO_2 nanoparticles in consideration of a porous film fulfilling a certain mechanical strength. The PD colloid is thus described as a blend consisting of encapsulated particles and dispersed TiO_2 nanoparticles.

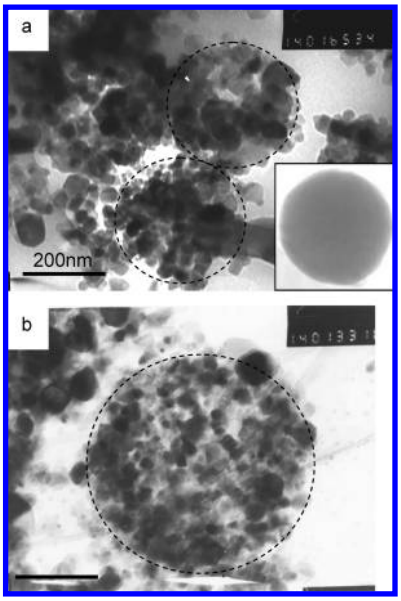

Figure 3. TEM pictures of the TiO_2-encapsulated polymer particle from (a) D1 and (b) D2 (The scale bars represent 200 nm). The inset of panel a shows a polymer particle before encapsulation.

The PD colloid was then coated onto the substrate by the technique of doctor-blading. The organic components and solvent were removed by thermal treatment at 450 °C, leaving the voids to form the porous film. It was reported that, in this kind of porous film constructed by TiO_2 nanoparticles, the tiny crystals (P25) interconnected to form a continuous network, through which charge carriers percolated across to the collecting contact. Charge transport in such mesoporous systems has been under intense investigation[30,31] and was best described by a random walk model.[32] On the boundary between the particles, electron transport occurs by diffusion, which was often the decisive step of the effective charge transport.[33] Therefore, the morphology of the porous film, which describes the way the particles are connected, plays an important role on the performance of the device.[34,35] Here, SEM was used to study the morphology of the calcinated film.

As shown in Figure 4, significant surface inhomogeneity together with bigger holes was observed for the films S1 and S2. These results indicate a clear alteration of the morphology for the films using PD colloid (Figure 4a,b) relative to the reference film (Figure 4c), where rather homogeneous films with uniform particle aggregates and smaller pores were obtained. Along with the size of the polymer particles in PD colloid increasing, the pores in S1 and S2 change accordingly. For S1, pores of several hundred nanometers in diameter are normally observed on the surface (Figure 4a), whereas, for S2 (Figure 4b), the pores become larger approaching to micrometer scale. The further quantitative investigation was performed by Brunauer−Emmett−Teller (BET) analysis.

(29) Shi, Y. T.; Zhan, C.; Wang, L. D.; Ma, B. B.; Gao, R.; Zhu, Y. F.; Qiu, Y. *Phys. Chem. Chem. Phys.*, 2009, DOI: 10.1039/b901003c.

(30) Hagfeldt, A.; Grätzel, M. *Acc. Chem. Res.* **2000**, *33*, 269–277.
(31) Hilgendorff, M.; Spanhel, L.; Rothenhäsuler, Ch.; Müller, G. *J. Electrochem. Soc.* **1998**, *145*, 3632–3637.
(32) Nelson, J. *Phys. Rev. B* **1999**, *59*, 15374–15380.
(33) Enright, B.; Fitzmaurice, D. *J. Phys. Chem. B* **1997**, *100*, 1027.
(34) Park, N. G.; van de Lagemaat, J.; Frank, A. J. *J. Phys. Chem. B* **2000**, *104*, 8989–8994.
(35) Cass, M. J.; Qiu, F. L.; Walker, A. B.; Fisher, A. C.; Peter, L. M. *J. Phys. Chem. B* **2003**, *107*, 113–119.

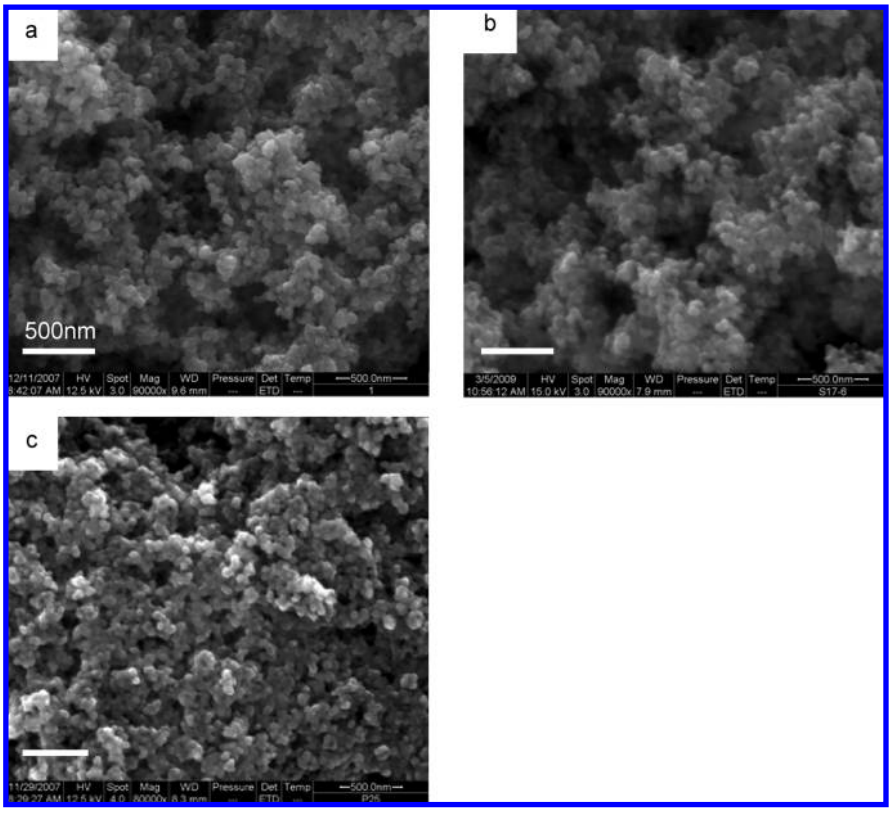

Figure 4. The SEM pictures of the porous TiO_2 film: (a) S1, (b) S2, and (c) the reference film. The scale bar is 500 nm.

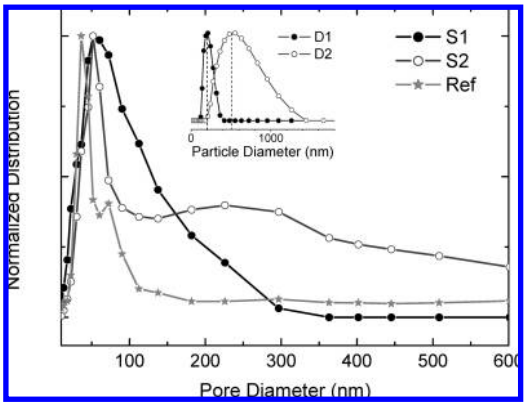

Figure 5. Pore size distribution of S1 (solid circle), S2 (hollow circle), and the reference (solid pentacle). The inset shows the particle size distribution in D1 and D2.

The BET analysis using mercury as the medium showed significantly increased values of the characteristic pore size for S1 and S2 in comparison with the reference film. It is clearly shown in Figure 5 that S1 and S2 possess a peak value of 50 nm. This is larger than the corresponding value of 36 nm for the reference film, which is similar to the previously reported value.[36] Furthermore, a broader peak is observed for S1 and S2. The porous structure of S1 has a size distribution ranging from 10 to 300 nm and S2 from 10 nm to larger than 1 μm, both are wider than the reference, which ranges from 10 to 100 nm. This result reveals a loose structure of S1 and S2, namely, the reference film has the finest porous structure.

The varied porous structure can be correlated to the different pore-forming agents adopted in the colloid. In the case where pores are produced by the pore-forming agent PEG, the pore formation mechanism could be illustrated as follows: The reference colloid is composed of TiO_2 particles well dispersed in PEG aqueous solution matrix. During film formation through doctor-blading on glass substrates, the PEG solution is concentrated due to water evaporation, and the TiO_2 particles continue to aggregate until the PEG concentration reaches c^* (the critical overlap concentration). The distance between TiO_2 particles is frozen then, which is expected to form pores after calcination. The pore size is determined by the size of gelated PEG solution between TiO_2 particles at the concentration of c^*. Therefore, it is easy to conclude that the pore size distribution is determined by many factors such as the volume ratio of TiO_2 particles and PEG, molecular weight of PEG, etc. Since PEG dissolves in water at the molecular level, the pores show very narrow distribution in size. However, it is difficult to flexibly control the pore size and the porous structure. Contrastively, the pores in S1 and S2 are formed by the different aggregates of polymer particles. This indicates that the pore size could be accurately tuned by modifying the particle size and the dispersibility of polymer particles. The ideal case is that the pore might be exactly equal in size to the particles in the PD. This was observed in our experiments. The particles in D1 are from 100 to 350 nm, which perfectly coincides with the pore size distribution of S1. For D2, the particles are from 200 nm to larger than 1 μm, being comparable to the pores in S2.

The big pores in S1 and S2 are expected to facilitate diffusion of electrolyte into the porous film. The porosity decided by BET is higher than 80% for S1 and S2, while the value is 62% for the reference cell.[37] Since TiO_2 films have the same thickness of

(36) Wang, P.; Wang, L. D.; Ma, B. B.; Li, B.; Qiu, Y. *J. Phys. Chem. B* **2006**, *110*, 14406–14409.

(37) Nazeeruddin, M. K.; Pechy, P.; Renouard, T.; Zakeeruddin, S. M.; Humphry-Baker, R.; Comte, P.; Cevey, L.; Costa, E.; Shklover, V.; Spiccia, L.; Deacon, G. B.; Bignozzi, C. A.; Grätzel, M. *J. Am. Chem. Soc.* **2001**, *123*, 1613–1624.

Table 1. Summarized Characteristics of the TiO_2 Film and the Corresponding Device

TiO_2 film	S1	reference
pore forming agent	PS-PBA dispersion, ø200 nm	PEG, 2×10^4 and 2×10^6g/mol
pore size distribution	10−300 nm	10−100 nm
porosity	0.86	0.62
adsorbed dye	4.6×10^{-8}mol/cm^2	12.6×10^{-8}mol/cm^2
haze factor	0.88	0.75
$R_{TiO2/Dye/EL}$	15 Ω	32 Ω
ff	0.65	0.60
Isc	10.6 mA/cm^2	11.7 mA/cm^2
Isc/Abs. Dye	2.3×10^8 mA/mol	0.9×10^8 mA/mol
normalized per-weight-efficiency	2.7	1

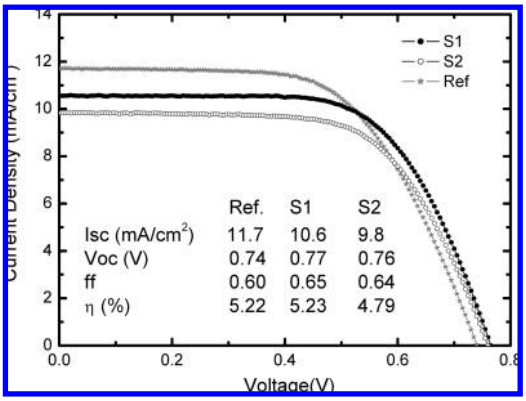

Figure 6. *I*−*V* curve of the device using different TiO_2 anodes: S1 (●); S2 (○), and reference (★).

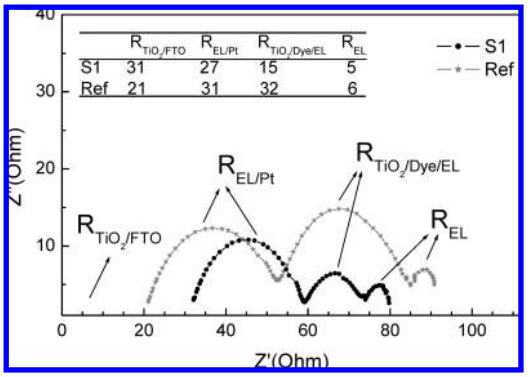

Figure 7. Impedance spectra of the studied device under illumination of AM1.5G.

10 μm, the high porosity indicates a less amount of TiO_2 contained in S1 and S2, which is not favorable for DSC because of the limitation of monolayer adsorption of dyes. A desorption experiment was carried out on the TiO_2 porous film with an area of 2.5×1.8 cm. The average amount of adsorbed dye was calculated to be 4.6×10^{-8} mol/cm^2 for S1, 7.99×10^{-8} mol/cm^2 for S2, and 12.56×10^{-8} mol/cm^2 for the reference film. As expected, S1 absorbs only 36% of the reference cell, and S2 absorbs 63% of the reference cell.

The photovoltaic response of the TiO_2 film was examined by fabricating a qausi-solid-state DSC using the film as a photoanode (Figure 6). When illuminated with simulated solar light of AM 1.5G with the incident light intensity of 100 mW/cm^2, the device based on S1 displays a short circuit current (Isc) of 10.6 mA/cm^2, an open circuit voltage (Voc) of 0.77 V, a fill factor (ff) of 0.65, and an efficiency of 5.23%. In comparison, the reference device shows an Isc of 11.7 mA/cm^2, a Voc of 0.74 V, an ff of 0.60, and an efficiency of 5.22%. The device based on S2 has an overall efficiency of 4.79%, lower than S1, indicating that the porous structure of S1 fulfills a better DSC than S2.

It has to be noted that the fill factor of S1 (ff = 0.65) is higher than that of the reference cell (ff = 0.60). Similar phenomena was observed in Kang's work, where an ff of 0.58 was obtained for a device based on a polymer-bead-modified solar cell, and 0.55 for the reference cell.[38] Furthermore, the Isc of S1 is comparable to that of the reference cell although S1 absorbs only 36% dyes of the latter. This indicates a higher photocurrent produced by per unit of dye for S1, which is 2.3×10^8 mA/mol, as listed in Table 1. Comparatively, the value of Isc/Abs.Dye is only 0.9×10^8 mA/mol for the reference cell.

In order to reveal the improvement, EIS was performed on the fabricated device. Under the full illumination, the Nyquist plot (Figure7) shows three semicircles in the measured frequency range of 0.05 Hz to 100 kHz. As reported in such DSC, the three semicircles are attributed to the redox reaction at the platinum counter electrode ($Z_{EL/Pt}$), the electron transfer at the TiO_2/dye/electrolyte interface ($Z_{TiO2/dye/EL}$), and carrier transport by ions within the electrolyte (Z_{EL}).[39,40] The resistance element $R_{EL/Pt}$, $R_{TiO2/dye/EL}$, and R_{EL} are described as the real part of $Z_{EL/Pt}$, $Z_{TiO2/dye/EL}$, and Z_{EL}, respectively.

The resistance in the high frequency range (left side in Nyquist plot) is influenced by the sheet resistance of FTO and the contact resistance between FTO and TiO_2 ($R_{FTO/TiO2}$). This value is larger for S1, implying that the section area of TiO_2 film is smaller. Since the porosity of S1 is higher, it contains smaller amount of TiO_2 nanoparticles at the same thickness as the reference film. This results in a loose porous structure and a smaller section area of S1, thus producing a high $R_{FTO/TiO2}$. However, the value of $R_{TiO2/dye/EL}$ for S1 is much smaller than that for the reference cell, indicating that the effective interfacial area between TiO_2 and electrolyte is larger for S1. Since the electrolyte used in this work is in quasi-solid-state and the viscosity is high (522 Pa·s), its diffusion into the porous structure of TiO_2 film could benefit from the big pores in S1. The optimized diffusion thus produces a closer contact between the porous structure and the electrolyte, resulting in a larger interfacial area. The further improvement on electron injection from dye to TiO_2 in the region close to bottom is also expected, which leads to a shorter electron path length. The overall effects produce a smaller $R_{TiO2/dye/EL}$ for S1. R_{EL} and $R_{EL/Pt}$ are similar since both devices adopt the same architecture. On a whole, a decreased interfacial resistance is observed for S1 relative

(38) Kang, S. H.; Kim, J. Y.; Kim, H. S.; Koh, H. D.; Lee, J. S.; Sung, Y. E. *J. Photochem. Photobiol. A: Chem.* **2008**, *200*, 294–300.

(39) Koide, N.; Islam, A.; Chiba, Y.; Han, L. *J. Photochem. Photobiol. A: Chem.* **2006**, *182*, 296–305.

(40) Ito, S.; Zakeeruddin, S. M.; Comte, P.; Liska, P.; Kuang, D.; Grätzel, M. *Nat. Photonics* **2008**, *2*, 693–698.

to the reference cell, which is expected to contribute to a more efficient electron collection.

The big pores in S1 can further function as scattering centers for enhancing light absorption. This was observed in transmission spectroscopy of TiO_2 film without dye adsorption or electrolyte. The result is characterized by the parameter of haze factor. The haze factor is well-known as an index of transparent conductive oxide (TCO) substrates for light scattering in the field of thin-film solar cells,[41] and was recently reported to investigate the optical path length in DSC.[39] It is defined as the ratio of the diffused light to the total light transmitted through the electrodes. The haze factor is calculated to be 75% for the reference cell and 88% for S1. This indicates that the prolonged average path length of the photon by light scattering effect is realized in S1, which enhances the light absorption ability, thus contributing to the improved photon-to-electron conversion efficiency.

To conclude, although S1 absorbs 36% photons of the reference cell due to the high porosity, the more efficient photon-to-electron conversion efficiency per unit of TiO_2 is obtained for S1 because of the decreased interfacial resistance and enhanced light scattering effect. The high per-weight-efficiency of S1 suggests that it has great potential to develop the performance of the quasi-solid-state DSC by adoption of PD. An optimized architecture of the device can also supply additional space for optimization. One way is to increase the thickness of the porous film. The advantage is that it is easy to realize, and the enhancement of light absorption accelerates the improvement at the same time. However, the thickness is limited by the electron diffusion ability of TiO_2. Therefore, an optimal thickness exists to balance the two sides. Further investigation is carried out in our lab.

(41) Meier, J.; Spitznagel, J.; Kroll, U.; Bucher, C.; Fay, S.; Moriarty, T.; Shah, A. *Thin Solid Films* **2004**, *518*, 451–452.

Conclusion

In summary, for the first time, a PD containing a copolymer of styrene and butyl acrylate was used in the preparation of a porous anode for DSCs. The quasi-solid-state DSC shows an improved per-weight-efficiency by a factor of 2.7 compared with the reference cell. This offers specific benefits of PD-based colloids over the reference colloid system. Further optimization could be potentially realized by optimal design of the cell structure. The low density of the photoanode is also expected to reduce the raw material cost. To be noted is that the stability of the PD colloid is much better than the reference colloid. The film forming ability of the latter declines as a result of the evaporation of the organic components, such as acetylacetone, during storage. The good stability facilitates the PD system for production on large scale. Furthermore, the work opens the gate for a technique of porous film with flexible controllability. By using a suitable PD, the desired porous structure can be easily obtained. This is not only applicable for quasi-solid-state DSC, but for all-solid-state DSC as well. Since the latter is environmental-friendly, the technique developed in this paper is promising to serve for green industry.

Acknowledgment. This work is supported by the China Postdoctoral Science Foundation (No. 20080430371), National Natural Science Foundation of China (No. 50873055 and 50802050), and National Key Basic Research and Development Programme of China (No. 2006CB806203 and 2009CB930602).